Clays and Clay Minerals, Vol. 46, No. 1, 38–50, 1998.

XRD MEASUREMENT OF MEAN THICKNESS, THICKNESS DISTRIBUTION AND STRAIN FOR ILLITE AND ILLITE–SMECTITE CRYSTALLITES BY THE BERTAUT–WARREN–AVERBACH TECHNIQUE

V. A. DRITS,[1] D. D. EBERL[2] AND J. ŚRODOŃ[3]

[1] Institute of Geology RAN, Pyzhevsky 7, 109017 Moscow, Russia

[2] U.S. Geological Survey, 3215 Marine St., Boulder, Colorado 80303-1066

[3] Institute of Geological Sciences PAN, Senacka 1, 31002 Krakow, Poland

Abstract—A modified version of the Bertaut–Warren–Averbach (BWA) technique (Bertaut 1949, 1950; Warren and Averbach 1950) has been developed to measure coherent scattering domain (CSD) sizes and strains in minerals by analysis of X-ray diffraction (XRD) data. This method is used to measure CSD thickness distributions for calculated and experimental XRD patterns of illites and illite–smectites (I–S). The method almost exactly recovers CSD thickness distributions for calculated illite XRD patterns. Natural I–S samples contain swelling layers that lead to nonperiodic structures in the c^* direction and to XRD peaks that are broadened and made asymmetric by mixed layering. Therefore, these peaks cannot be analyzed by the BWA method. These difficulties are overcome by K-saturation and heating prior to X-ray analysis in order to form 10-Å periodic structures. BWA analysis yields the thickness distribution of mixed-layer crystals (coherently diffracting stacks of fundamental illite particles). For most I–S samples, CSD thickness distributions can be approximated by lognormal functions. Mixed-layer crystal mean thickness and expandability then can be used to calculate fundamental illite particle mean thickness. Analyses of the dehydrated, K-saturated samples indicate that basal XRD reflections are broadened by symmetrical strain that may be related to local variations in smectite interlayers caused by dehydration, and that the standard deviation of the strain increases regularly with expandability. The 001 and 002 reflections are affected only slightly by this strain and therefore are suited for CSD thickness analysis. Mean mixed-layer crystal thicknesses for dehydrated I–S measured by the BWA method are very close to those measured by an integral peak width method.

Key Words—Crystallite, Fundamental Illite Particles, Illite, Illite–Smectite, MacEwan Crystallites, Mixed-Layer Clay, Thickness Distributions, Warren–Averbach Method.

INTRODUCTION

The BWA technique (Bertaut 1949, 1950; Warren and Averbach 1950) analyzes profiles of XRD reflections and permits determination of the area-weighted mean size of CSDs (also referred to as "crystallites"), the distribution of these sizes and fluctuations in the *d*-spacings (microstrains) of the CSDs. This method, based on Fourier analysis, has been applied widely to metals and alloys, but until recently (Eberl and Środoń 1988; Árkai et al. 1996) has not been applied to minerals, except for the work of Kodama (1965) and Kodama et al. (1971), devoted mainly to the analysis of microstrain in fine-grained dioctahedral micas. The CSD size and size distribution are essential characteristics of the real crystal structure of a mineral. For example, the mean thickness and thickness distribution of illite and I–S CSDs could serve as indicators of the degree of diagenesis and of low-grade metamorphism.

Eberl and Środoń (1988) were the first to apply the BWA approach to the study of mixed-layer I–S samples, utilizing the Siemens Corporation D5000 software (Siemens 1990). This application was not completely appropriate for I–S studies, because the BWA method was developed for periodic crystals. Eberl and Blum (1993) tried to solve this problem by saturating the smectite interlayers with either Ca or Sr cations to obtain 15-Å water–clay complexes. Alternation of 15-Å smectite and 10-Å illite layers preserves the coherency of the waves scattered in the direction of the diffraction maximum, with d = 5.0 Å. Therefore, Fourier analysis of this reflection should yield the parameters of interest. However, subsequent results (unpublished data) have indicated that the 15-Å complex was not completely developed for many of their samples.

Recently, Lanson and Kubler (1994) used the same technique and the same software to analyze profiles of basal reflections for a large collection of illites and I–S. For some samples they found a strong disagreement among mean thicknesses of CSDs obtained by Fourier analysis and by other techniques. These authors concluded that, in its standard form, the method cannot be applied to the study of illite and I–S.

In the course of further experiments with the commercial BWA software, we realized that some of the information contained in the peak profile was lost when mathematical functions were fitted to the experimental data prior to Fourier analysis. We then decided to develop our own program (Eberl et al. 1996) to avoid this and other simplifications. In the present paper, we describe the theory on which the program is based, and

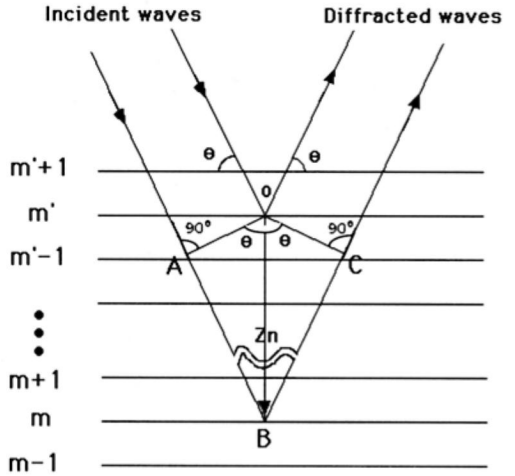

Figure 1. A schematic illustrating the difference in paths traveled by diffracted waves scattered by m′ and m layers separated by n interlayer spacings ($n = m' - m$), so that the distance between the layers $Z_n = m'd(001) - md(001) = nd(001)$.

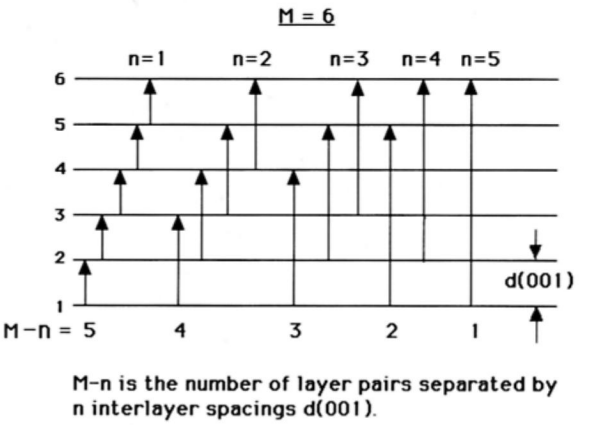

Figure 2. Relation between total number of layers in a crystal (M) and amount of pairs of layers ($M - n$) separated by n spacings of $d(001)$. An increase in n from 1 to 5 decreases the number of nth neighbors from 5 to 1.

application of this program to the study of clay minerals, with particular reference to illite and I–S.

THEORY OF THE BWA TECHNIQUE

The treatment presented below follows the original works of Bertaut (1949, 1950) and Warren and Averbach (1950), but it is simplified for the analysis of basal reflection profiles. We have simplified the equations by eliminating constants which do not affect the shape of 00l reflections. We use the term "CSD" for a stack of layers parallel to each other.

Experimental Determination of the Interference Function

The intensity distribution $I(2\theta)$ for a 00l reflection of a layered mineral, consisting of CSDs with a strict periodicity along the c^* axis, can be written as:

$$I(2\theta) = \mathrm{Lp}(2\theta)G^2(2\theta)\phi(2\theta) \quad [1]$$

Lp(2θ) is a combination of the Lorentz and polarization factors which accounts for intensity contributions due to X-ray beam polarization, and for geometrical factors related to the volume and orientation of crystals in the X-ray beam (Reynolds 1986; Moore and Reynolds 1989). $G^2(2\theta)$ is the structure factor that represents diffraction from the arrangement of atoms within the unit cell. The symbol $\phi(2\theta)$ is the interference function, which depends on the thickness of CSDs, the thickness distribution and the microstrains or layer spacing fluctuations.

The values of Lp(2θ) and $G^2(2\theta)$ can be calculated *a priori* if experimental conditions for diffraction and chemical and structural data for the mineral under study are well known. These functions are not sensitive to CSD sizes and microstrains. Therefore, we can limit consideration to the interference function:

$$\phi(2\theta) = \frac{I(2\theta)}{\mathrm{Lp}(2\theta)G^2(2\theta)} \quad [2]$$

It is convenient to replace the 2θ variable of XRD patterns with a new continuous variable, Z^*, along the c^* axis in reciprocal space. The values of Z^* are related to the corresponding 2θ values by the equation:

$$Z^* = 2 \sin \theta/\lambda \quad [3]$$

where λ is the wavelength of the radiation and θ is a continuous variable.

Physical Meaning of the Interference Function

The interference function represents effects of the phase differences that appear during wave scattering by all the nth nearest layer pairs that exist in CSDs. To make this clear, let us consider first a sample where CSDs have the same thickness and consist of M identical layers (Figure 1). Let us consider 2 layers, m' and m, separated by $n = m' - m$ interlayer spacings $d(001)$. The paths traveled by waves scattered by these 2 layers differ by the length $\Delta = (AB + BC) = 2Z_n \sin \theta$, where $Z_n = nd(001)$ and θ is the angle between the initial X-ray beam and (001) planes (Figure 1). The phase difference (ρ) between the waves is related to Δ:

$$\rho = \frac{2\pi}{\lambda}\Delta = 2\pi Z_n \frac{2 \sin \theta}{\lambda} = 2\pi Z_n Z^* \quad [4]$$

This phase difference contribution to diffraction is expressed by a cos $2\pi Z_n Z^*$ term (James 1965).

The value of $(M - n)$ gives the number of layer pairs separated by n interlayer spacings that exist in the CSD. This relationship is illustrated in Figure 2. The product:

$$(M - n)\cos 2\pi Z_n Z^* \quad [5]$$

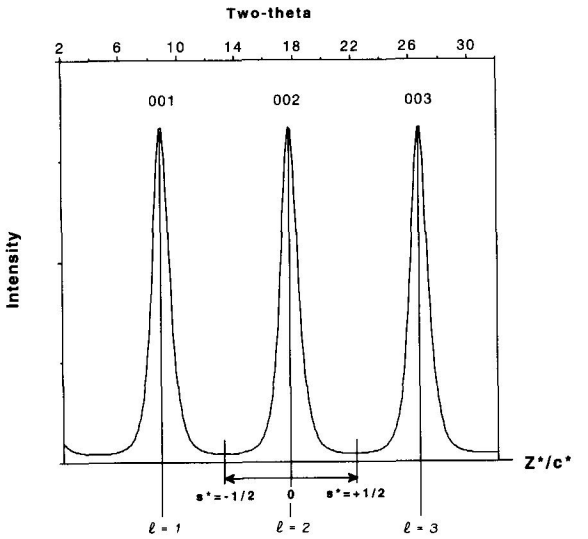

Figure 3. $00l$ peaks of the interference function located along the Z^*/c^* axis. For the 002 peak, the origin is chosen at its maximum so that a new variable s^* may vary from $-½$ to $+½$ $Z^*/c^* = l + s^*$.

represents the effect of the difference in phase of waves scattered by all the nth nearest layer pairs in a CSD of a given M. The summation of these products for all $|n| = |m' - m|$ (that is, for $n = m' - m$ and $-n = m - m'$), normalized for the unit cell (that is, divided by M), gives the interference function, $\phi(Z^*)$, which describes the total effect of the phase difference on the intensity distribution along the Z^* axis:

$$\phi(Z^*) = \sum_{n=-M}^{M} \frac{(M - |n|)}{M} \cos 2\pi Z_n Z^* \qquad [6]$$

It is physically unrealistic to assume that samples consist of CSDs having the same number of layers. Therefore, let us consider a sample that consists of CSDs with a distribution of thicknesses defined by $f(M)$, so that:

$$\sum_{M_1}^{M_2} f(M) = 1 \quad \text{and} \quad \sum_{M_1}^{M_2} Mf(M) = \overline{M} \qquad [7]$$

where M_1 and M_2 correspond to CSDs having the smallest and the largest number of layers respectively and $\overline{M}$ is the mean number of layers per CSD.

The number of nth nearest layer pairs in all CSDs consisting of M layers is equal to $f(M)(M - n)$. Since CSDs have different thicknesses, the mean number of layer pairs separated by n interlayer spacings is:

$$N(n) = \sum_{M_1}^{M_2} (M - n)f(M) \qquad [8]$$

If we replace $(M - |n|)$ and M in Equation [6] by $N(n)$ and $\overline{M}$, respectively, we will obtain the interference function for samples having a distribution of CSD thicknesses:

$$\phi(Z^*) = \sum_{n=-M_2}^{M_2} \frac{N(n)}{\overline{M}} \cos 2\pi Z_n Z^* = \sum_{n=-M_2}^{M_2} H(n) \cos 2\pi Z_n Z^* \qquad [9]$$

where:

$$H(n) = \frac{1}{\overline{M}} \sum_{M_1}^{M_2} (M - n)f(M) \qquad [10]$$

The interference function represents a series of bell-like peaks of identical shape, located along the Z^* axis at positions corresponding to $00l$ reflections (Figure 3).

The Interference Function as a Fourier Series

Let us replace the absolute Z^* coordinate by the fractional coordinate Z^*/c^*, that is, express it in terms of a fraction of the reciprocal unit cell parameter $c^* = 1/d(001)$. Then positions of intensities along the Z^* axis for each $00l$ reflection (defined as each $00l$ interference function peak) may be expressed as:

$$Z^*/c^* = Z_l^*/c^* + s^* = l + s^* \quad \text{where } 1 \geq s^* \geq 0 \qquad [11]$$

where $Z_l^* = 2 \sin \theta_l/\lambda = l/d(001)$ is the coordinate corresponding to the Bragg law position for a $00l$ reflection and s^* is a new variable parameter.

Let us now treat each peak separately and choose the origin of the coordinate for each individual $00l$ reflection at the position of its maximum, that is, setting $l = 0$. In this case, s^* values within a $00l$ reflection are limited by an interval from $-½$ to $½$ (Figure 3) and:

$$Z_n Z^* = nd(001)c^*s^* = ns^* \qquad [12]$$

Thus:

$$\phi(Z^*) = \phi(s^*) = \sum_{n=-M_2}^{M_2} H(n) \cos 2\pi n s^* \qquad [13]$$

Because n is an integer, the interference function represents a Fourier series. The Fourier coefficients $H(n)$ are obtained by the back Fourier transformation of $\phi(s^*)$, that is:

$$H(n) = \sum_{s^*=-1/2}^{1/2} \phi(s^*) \cos 2\pi n s^* \qquad [14]$$

Determination of $f(M)$ and $\overline{M}$

$H(n)$ is a function dependent on the mean thickness and the thickness distribution of CSDs. It follows from Equation [10] that:

$$\left.\frac{\partial H(n)}{\partial n}\right|_{n\to 0} = \frac{1}{\overline{M}}, \quad \text{and} \quad \left.\frac{\partial^2 H(n)}{\partial n^2}\right|_{n\to 0} = \frac{f(M)}{\overline{M}} \qquad [15]$$

The thickness T of a CSD is $T = Md(001)$. In the case

of illite, $d(001) = 1$ nm, so $T = M$ nm. Thus, the first derivative of $H(n)$ at $n \approx 0$ determines the mean thickness of CSDs ($\overline{T}$) and the second derivative gives the CSD thickness distribution.

Fluctuations in the Position of Layers

A periodic structure of CSDs may be disturbed due to slight fluctuations in the layer thicknesses. To any pair of the nearest layers ($n = 1$) separated by the distance Z_1, one can associate a variation ϵ_1 with respect to the ideal value $d(001)$. This ϵ_1 variable may vary from one pair of layers to another and the variation of Z_1 may be described by a statistical distribution function, $\gamma_1(Z)$. In the general case of nth nearest neighbors, we have the general relation:

$$Z_n = nd(001) + \epsilon_n = (n + \delta_n)d(001) \quad [16]$$

where ϵ_n is the difference between the ideal distance and the true distance and δ_n is the same parameter expressed as a fraction of $d(001)$. The variable ϵ_n may vary for each pair of the nth nearest neighbors and the variation of Z_n may be described by a statistical distribution function $\gamma_n(Z_n)$ (Guinier 1964; Drits and Tchoubar 1990). Because of the spacing fluctuations, the cosine terms in Equation [9] must be averaged over all possible Z_n values for each given n. Thus, the mean phase difference of waves diffracted by all layer pairs separated by different interlayer spacings may be written as:

$$\phi(Z^*) = \sum_{n=-M_2}^{M_2} H(n)\overline{\cos 2\pi Z_n Z^*} \quad [17]$$

Using Equations [11] and [16], the product Z_nZ^* may be modified as:

$$Z_nZ^* = (n + \delta_n)d(001)(l + s^*)c^* = nl + ns^* + l\delta_n \quad [18]$$

because $c^* = 1/d(001)$ and we have neglected the $\delta_n s^*$ term, since $\delta_n \ll 1$ and $s^* < 1$. Then:

$$\begin{aligned}\overline{\cos 2\pi Z_n Z^*} &= \overline{\cos 2\pi(ns^* + l\delta_n)} \\ &= \cos 2\pi ns^* \overline{\cos 2\pi l\delta_n} \\ &\quad - \sin 2\pi ns^* \overline{\sin 2\pi l\delta_n} \end{aligned} \quad [19]$$

because the mean applies only to terms containing δ_n and $\cos(nl + ns^*) = \cos(ns^*)$, nl being an integer. Equation [17] then can be presented as:

$$\phi(s^*) = \sum_{-\infty}^{\infty} A(n)\cos 2\pi ns^* - \sum_{-\infty}^{\infty} B(n)\sin 2\pi ns^* \quad [20]$$

where:

$$A(n) = H(n)\overline{\cos 2\pi l\delta_n} \quad \text{and} \quad B(n) = H(n)\overline{\sin 2\pi l\delta_n} \quad [21]$$

As was mentioned, every pair of layers, m' and m, enters into summation twice as $n = m' - m$ and $-n = m - m'$. Since $\delta_n = \delta_{m'} - \delta_m$ and $-\delta_{-n} = \delta_m - \delta_{m'}$, it follows that $\delta_n = \delta_{-n}$; hence, after summation, the sine terms in Equation [20] vanish:

$$\phi(s^*) = \sum_{-\infty}^{\infty} A(n)\cos 2\pi ns^* \quad (22)$$

Again $\phi(s^*)$ has a form of the Fourier series and the $A(n)$ coefficients may be determined from the experimental profile of a $00l$ reflection by the equation:

$$A(n) = \sum_{s^*=-1/2}^{1/2} \phi(s^*)\cos 2\pi ns^* \quad [23]$$

As can be seen from Equation [10], the size term, $H(n)$, is independent of l, whereas the $\overline{\cos 2\pi l\delta_n}$ term depends upon the reflection order. Therefore, using $A(n)$ one may determine $H(n)$ and fluctuations in layer positions if at least two $00l$ reflections are analyzed.

In order to obtain the precise mean values of the cosine terms in Equation [21] we must know the distribution law for the deviation, ϵ_n or δ_n. The simplest assumption is that this distribution follows the Gaussian function:

$$\gamma(\epsilon) = \frac{1}{\sqrt{2\pi}\sigma}\exp -\left(\frac{\epsilon^2}{2\sigma^2}\right) = \frac{1}{\sqrt{2\pi}\sigma}\exp -\left\{\frac{\delta^2 d^2(001)}{2\sigma^2}\right\} \quad [24]$$

in which $\sigma = (\overline{\sigma^2})^{1/2} = (\overline{\epsilon^2})^{1/2} = (\overline{\delta^2})^{1/2}\, d(001)$ is the standard (or root mean square) deviation equal to the half-width at half-maximum of the strain distribution, $\gamma(\epsilon)$, divided by $(2 \ln 2)^{1/2}$. First one must take into account the fluctuations in layer positions of all nearest layer pairs. In order to do this, one has to sum $\gamma(\delta_1)\cos 2\pi l\delta_1$ for any possible values of δ_1, where $\gamma(\delta_1)$ is the probability to find δ_1. Thus:

$$\begin{aligned}&\overline{\cos 2\pi l\delta_1} \\ &= \frac{1}{\sqrt{2\pi}\sigma_1}\int_{-\infty}^{\infty} \cos 2\pi l\delta_1 \exp(-\delta_1^2 d^2(001)/2\sigma_1^2)\, d\delta_1 \\ &= \exp -\left[\frac{2\pi^2 l^2 \overline{\sigma_1^2}}{d^2(001)}\right] \end{aligned} \quad [25]$$

where $\overline{\sigma_1^2} = (\overline{\delta_1^2})\overline{d^2(001)}$ is a variance of ϵ_1 or δ_1 or a mean square deviation of these values. As follows from Equation [21], we are interested in calculating $\overline{\cos 2\pi l\delta_n}$ for any n. The standard deviation of the distribution of ϵ_n is related to the standard deviation of nearest layer pairs as follows: $\overline{\sigma_n^2} = n\overline{\sigma_1^2}$ (Maire and Mering 1960; Reynolds 1989; Drits and Tchoubar 1990). Hence:

$$A(n) = H(n)\overline{\cos 2\pi l\delta_n} = H(n)\exp\left[-\frac{2\pi^2 l^2 n\overline{\sigma_1^2}}{d^2(001)}\right] \quad [26]$$

and

$$\ln A(n) = \ln H(n) - \frac{2\pi^2 l^2 n\overline{\sigma_1^2}}{d^2(001)} \quad [27]$$

If only 2 basal reflections, $00l_1$ and $00l_2$, are available, the $\overline{\sigma_1^2}$ value can be found analytically:

$$\overline{\sigma_1^2} = \frac{d^2(001)\ln[A_{l_1}(n)/A_{l_2}(n)]}{2\pi^2 n(l_2^2 - l_1^2)} \quad [28]$$

If ϵ_1 follows the Gaussian function, then $\overline{\sigma_1^2}$ does not depend on n.

Using Equation [23], the $A(n)$ values are found for each $00l$ reflection. Then, for a fixed value of n, a plot of the values for $\ln A(n)$ versus l^2 is constructed. The extrapolation to $l = 0$ gives $H(n)$ and the slope of the plot gives $-2\pi^2 n\overline{\sigma_1^2}/d^2(001)$. The value of $(\overline{\sigma_1^2})^{1/2}$ is the root mean square fluctuation of adjacent layer thicknesses in, for example, Å units.

In the general case, when the distribution law of ϵ_n is unknown, one may use an approach which is valid for small l and n values:

$$\overline{\cos 2\pi l\delta_n} \approx \left[1 - 4\pi^2 l^2 \overline{\delta_n^2}\right]^{1/2}$$
$$\approx 1 - 2\pi^2 l^2 \overline{\delta_n^2} \approx \exp -2\pi l^2 \overline{\delta_n^2} \quad [29]$$

The plot $\ln A(n)$ versus l^2 will be represented by straight lines only in the small n region, but this is just a region most suitable for a linear extrapolation to $l = 0$. This method does not require any assumption about the nature of layer thickness fluctuations. If $\overline{\delta_n^2}$ values determined by Equation [29] and divided by n lead to a constant value, it means that the distribution law corresponds to a Gaussian function (compare Equations [26] and [29]).

EXTRACTION OF THE INTERFERENCE FUNCTION FROM AN XRD PATTERN

The theoretical treatment presented above ignores experimental conditions that may affect the shapes of XRD peaks. These effects include background, overlapping of $K\alpha_1$ and $K\alpha_2$ peaks and instrumental broadening (Klug and Alexander 1974). We attempted to recover the interference function (which contains the particle size and strain information) from XRD peaks first by smoothing the XRD peak and removing the background, then by extracting the $K\alpha_1$ peak and deconvolving instrumental broadening and finally by extracting the interference function according to Equation [2].

This order of calculation proved unsuccessful: smoothing noise from the intensity data by using a moving average broadened the XRD peaks; the background intensity function could not be removed because its shape was unknown; instrumental broadening cannot be evaluated theoretically; and finding an appropriate instrumental standard for illite (a powdered mineral completely free from crystal size and strain broadening with a d close to the XRD peak to be analyzed) proved difficult. Finally, removing $\mathrm{Lp}(2\theta)G^2(2\theta)$ (hereafter referred to as $\mathrm{Lp}G^2$) by division according to Equation [2] often distorted the interference function so badly that it could not be used for crystallite size and strain analysis.

To circumvent these problems, a computer program (MudMaster; Eberl et al. 1996) was written using a calculation sequence that was optimized by trial and error to circumvent these problems. XRD patterns were recorded from 4.5-cm-long oriented clay preparations using a diffracted beam monochromator and relatively long count times (at least 5 s/0.02 °2θ step, with a tube current of 40 kV and 30 mA) to minimize background and noise, so that the intensity data did not require smoothing. An analytical range was chosen that was broad enough to encompass the complete range of the interference function peak (that is, halfway between the peaks of subsequent orders), so that little intensity was lost during background removal. A Siemens D500 diffractometer using incident and diffracted beam Söller slits, a 1° divergence slit and a relatively narrow receiving slit (0.15°) was employed to minimize instrumental broadening. An attempt was made to use the >20 μm size fraction of NITS SRM 675 synthetic fluorophlogopite as an instrumental standard. Deconvolution of instrumental broadening by the Stokes (1948) technique (Klug and Alexander 1974) yielded acceptable mean thicknesses for natural illites and I–S, but distorted crystallite thickness distributions for samples having mean thicknesses greater than about 15 nm. By comparison between samples run with and without the instrumental standard, instrumental broadening was found to be insignificant under our instrumental conditions for crystallite thicknesses <20 nm.

The values of G^2 for the illite unit cell were calculated using a program written by the authors (CALCLPG2) and atomic coordinates given by Moore and Reynolds (1989). To analyze NEWMOD©-calculated illite XRD patterns, potassium content (K) was determined as follows:

$$\text{equivalents K per half-unit cell} = 0.89[(\bar{T} - 1)/\bar{T}] \quad [30]$$

where $\bar{T}$ is the mean illite crystallite thickness in nm and 0.89 the charge of an illite interlayer per half-unit cell. This equation corrects K-content for the presence of crystal edges which, for NEWMOD©-calculated patterns, contain no K. For natural I–S, K-content was determined from the percentage of smectite interlayers (expandability, that is, %S) measured from glycolated samples (Środoń 1980; Środoń and Elsass 1994) prior to K-saturation and heating, assuming that the typical smectite layer charge is −0.4 equivalents/$O_{10}(OH)_2$. The relation is:

$$\text{equivalents K} = \frac{0.01(\bar{T} - 1)}{\bar{T}}[0.40(\%S) + 0.89(100 - \%S)] + \frac{0.4}{\bar{T}} \quad [31]$$

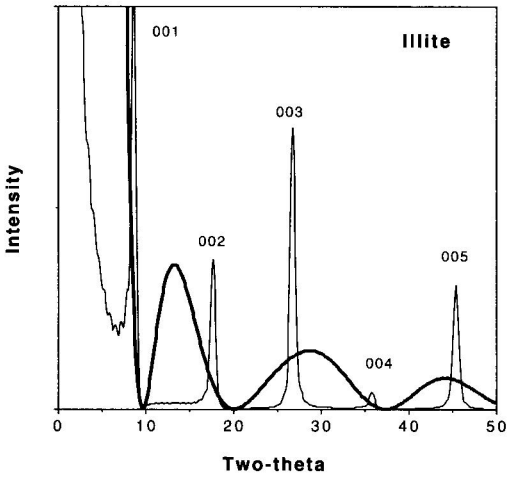

Figure 4. A NEWMOD©-calculated illite XRD pattern (thin line) and its LpG^2 (thicker line).

An Lp factor was used that combines the random and single-crystal Lp factors (Equation 3.13 in Moore and Reynolds 1989). However, use of the random Lp factor, of the single-crystal Lp factor or of Lp factors that were calculated for a different sample orientation and instrumental slit system did not significantly change the results.

LpG^2 of layer silicates is modulated and has approximately zero values at several 2θ angles (Figure 4). The interference function produced by division of the experimental XRD intensities (Figure 5A) by LpG^2 may be deformed near such angles (Figures 4 and 5B), because small inaccuracies in the estimation of LpG^2 or in the determination of background have a strong effect on the shape of the recovered interference function in these regions. For example values of LpG^2 are calculated for periodic crystals and therefore cannot take into account crystal end-effects which cause NEWMOD©-calculated and natural illite crystals to be slightly aperiodic. Therefore a technique was developed that relies on the fact that the interference function peaks are strictly symmetric (Figure 3). The undistorted half of the interference function peak is "flipped" over a vertical plane passing through the peak maximum (Figure 5C). For illites, 001, 002 and 004 reflections are flipped from low-2θ to high-2θ. The 003 and the 005 can be flipped in either direction if one side of a peak is deformed by mineral admixtures. After flipping, or if flipping is not applied, the residual background is removed by setting to zero the minima on either side of the interference function peak. Prior to flipping, the $K\alpha_2$ component to the interference function can be removed by a Fourier method (Gangulee 1970; Eberl et al. 1996).

The interference function peak (Figure 5C), so extracted from the XRD intensity data (Figure 5A), then was analyzed by the BWA technique as was described

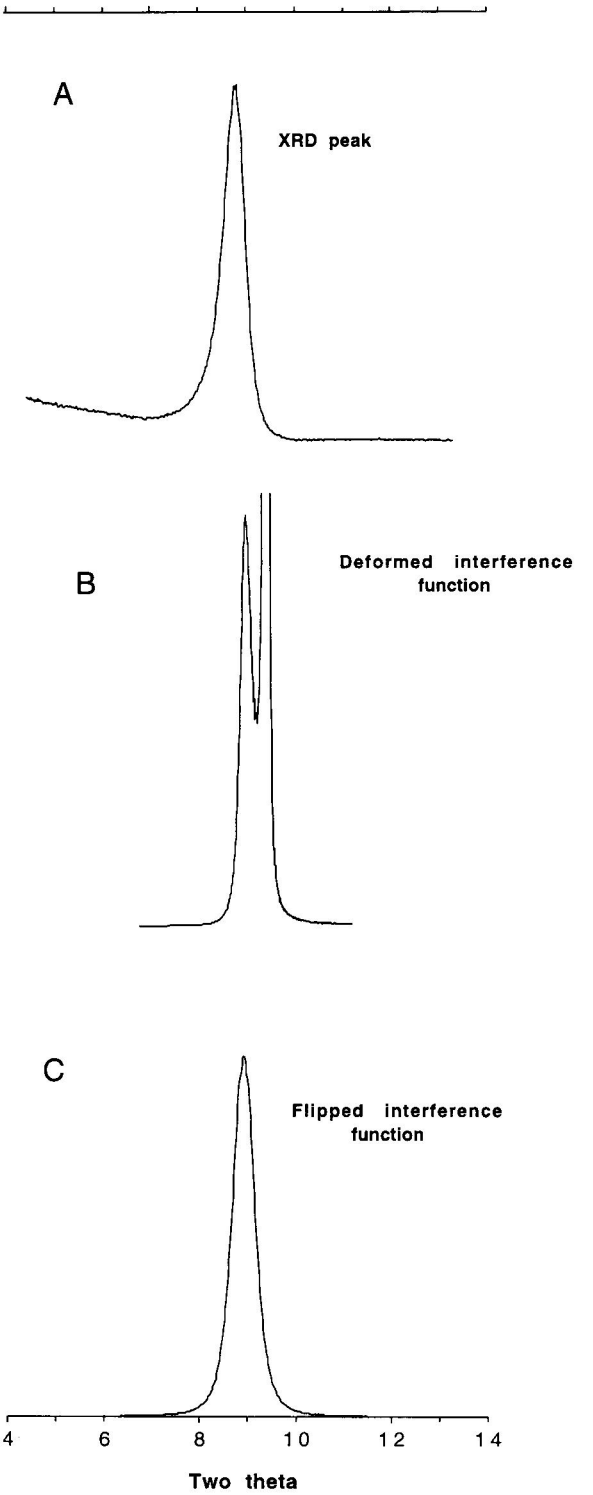

Figure 5. Patterns for K-saturated and dehydrated Zempleni sample, a 15% expandable $R > 1$ ordered I–S prior to dehydration. A = 001 XRD peak; B = interference function calculated by dividing the XRD intensities in A by LpG^2 for an illite with the appropriate chemical composition; C = final interference function to be analyzed by MudMaster, formed by flipping the left half of the peak in B from left to right.

Table 1. Parameters of crystal thickness distributions measured by the BWA and by the integral peak width (Drits et al. 1997) methods from XRD patterns of illites that were calculated using NEWMOD, with lognormal distributions of crystallite thickness having means of 5 and 20 layers.

Pattern & reflection	$\overline{T}_e$ (nm)	$\overline{T}_d$ (nm)	$\overline{T}_i$ (nm)	α	β^2	$Id(00l)$ (Å)
Lognor 5				input =1.51	input = 0.20	input = 9.98 Å
001	5.2	5.3	5.0	1.55	0.22	10.00
002	5.4	5.4	5.2	1.61	0.17	9.98
003	5.3	5.3	4.9	1.57	0.18	9.98
004	4.6	4.6	4.7	1.42	0.21	9.99
005	4.9	4.9	4.7	1.48	0.20	9.98
Lognor 20				input = 2.83	input = 0.34	input = 9.98 Å
001	19.7	20.2	20.2	2.84	0.33	9.98
002	20.4	20.5	18.6	2.87	0.30	9.98
003	20.1	20.0	18.5	2.83	0.35	9.98
004	19.9	19.9	17.9	2.83	0.32	9.98
005	19.7	19.7	18.4	2.81	0.34	9.98

Key: $\overline{T}_e$, $\overline{T}_d$, and $\overline{T}_i$, are mean thicknesses calculated from the first derivative of the Fourier coefficients plot, from the crystal thickness distribution (without smoothing, except for the Lognor 20, 001 reflection for which a smoothing power of 1 was used) and from the integral peak width method of Drits et al. 1997, respectively. The symbols α and β^2 are the lognormal parameters for the input distribution and for distributions calculated from the BWA method. The representation $d(001)$ is the position of the maximum of the interference function.

in the "Theory" section. Fourier coefficients $A(n)$ were calculated for each reflection from $n = 0$ to a maximum n equal to $5\overline{T}$ where $\overline{T}$ the mean number of illite layers in the crystallites. At this maximum n the frequency generally is less than 0.001 of the maximum frequency and therefore larger n's can be ignored. Fourier coefficients at small n's frequently are distorted due to loss of intensity during background removal and therefore must be corrected for the hook effect (Klug and Alexander 1974). Analysis of NEWMOD©-calculated illite XRD patterns indicates that the hook correction for the Fourier coefficients is best performed by extrapolating the steepest slope of the curve of $H(n)$ versus n to $H(n) = 0$ to find the mean thickness, and that the size distribution is best determined by taking the second derivative of the same curve not corrected for the hook effect (Equation [15]). The first and second derivatives of the Fourier coefficients can be smoothed, using a moving average of 3 or 5 (smoothing power = 1 or 2 in the MudMaster program) to decrease noise in the thickness distributions. The thickness distributions can be cut off at a designated thickness to eliminate ripples that may appear in the distribution at large thicknesses. If such ripples are present, the distribution is cut off at a size that makes the distribution mean approximately equal to the mean determined by extrapolation.

VERIFICATION USING NEWMOD©-CALCULATED XRD PATTERNS

To test the BWA technique incorporated in the program MudMaster, we analyzed XRD patterns that were calculated for a range of crystallite size distributions using NEWMODSKY, a version of NEWMOD© (Reynolds 1985) modified by R. C. Reynolds, Jr., to permit input of crystallite size distributions from an external file. Optimal input parameters for MudMaster for the hook correction, for the 2θ interval of the analysis, for smoothing conditions and for the maximum n to be used in the calculation were thereby were established, and were then used to study the more complicated XRD patterns of natural illites and I–S.

Most NEWMODSKY illite patterns were calculated using lognormal crystallite thickness distributions, because this distribution law is common to many minerals, including illite (Eberl et al. 1990; Drits et al. 1997). Two parameters, α and β^2, which correspond, respectively, to the mean value and the variance of ln T, where T is the crystallite thickness and $f(T)$ is the frequency of that thickness, characterize the distribution completely, where:

$$\alpha = \sum \ln Tf(T), \quad \text{and} \qquad [32]$$

$$\beta^2 = \sum [\ln T - \alpha]^2 f(T) \qquad [33]$$

Values of α, β^2 and $\overline{T}$ for 2 crystallite thickness distributions used to calculate NEWMOD© XRD patterns are compared with values extracted from the calculated XRD patterns by MudMaster (Table 1). The agreement is satisfactory. The best data are obtained if the interference function peaks can be recovered over the complete 2θ range, starting midway between neighboring $00l$ reflections. If the analytical range is narrower, $\overline{T}$ tends to be overestimated and β^2 underestimated.

NEWMOD© patterns having CSDs with a variety of shapes were calculated and then analyzed by MudMaster. Figure 6 illustrates that NEWMOD© inputs having equal (Figure 6A) and lognormal (Figure 6B) distributions can be recovered almost perfectly. A

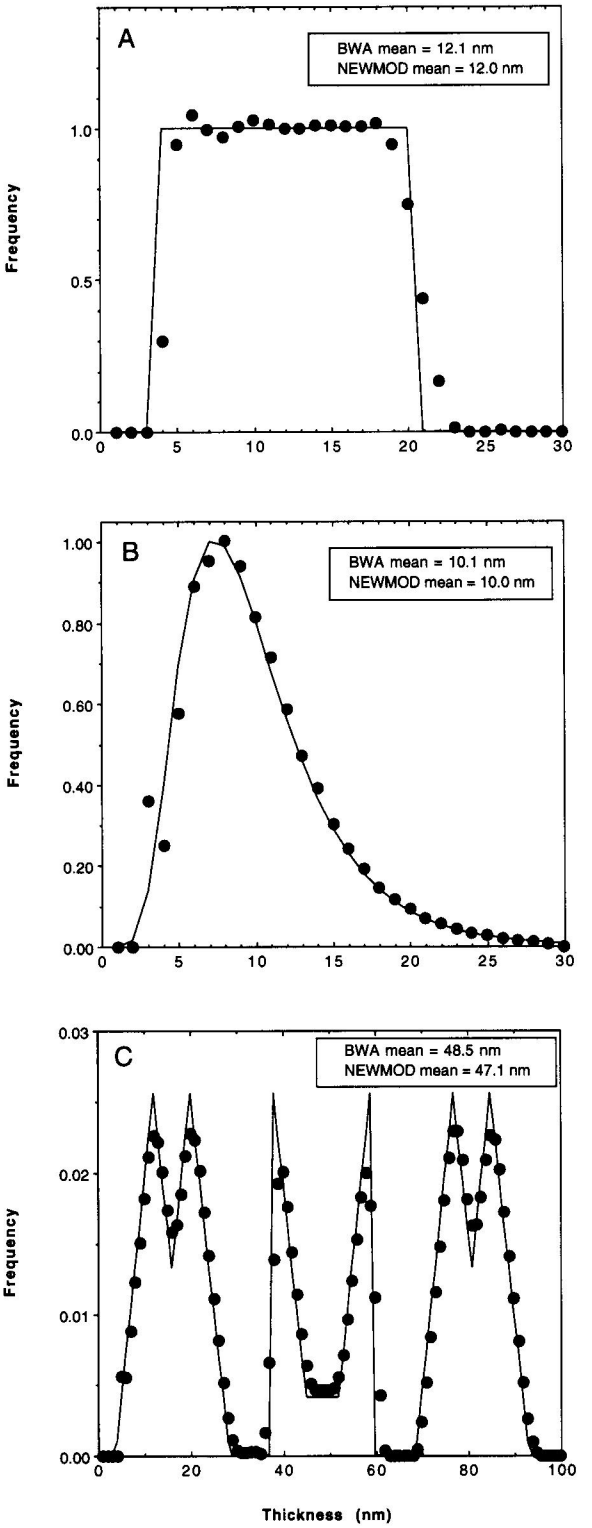

Figure 6. Crystallite size distributions used in NEWMOD© calculations of 003 illite XRD peaks (solid lines) compared with distributions recovered by MudMaster analysis of those peaks (dots). A = even distribution, from 4 to 20 layers (no smoothing); B = lognormal distribution having a mean of 10 layers (no smoothing); C = distribution spelling the word "MUM" (smoothing power of 1).

more complicated distribution that spells the word "MUM" was tested to see if the program can recover multimodal distributions. The $K\alpha_1 - K\alpha_2$ doublet was included in the pattern by adding NEWMOD© patterns calculated with $K\alpha_1$ and $K\alpha_2$ radiation in the proportion 2:1. The mean and the distribution were recovered almost perfectly (Figure 6C) from each of first 5 basal reflections, provided that the $K\alpha_2$ correction was applied to reflection orders greater than 1.

The effect of the $K\alpha_1 - K\alpha_2$ doublet on the BWA calculation was investigated for calculated illite patterns for illites having mean thicknesses ranging from 7 to 45 nm. The results indicate that $K\alpha_2$ need not be removed from the patterns, even for the 005 peak, if $\bar{T} < 20$ nm; but if $\bar{T} = 45$, distributions were distorted and the mean values were lowered for reflection orders greater than the 001 if $K\alpha_2$ was not removed.

These studies of synthetic XRD patterns indicate that, if applied correctly, the BWA method is capable of reproducing almost perfectly the original crystallite thickness distributions used in calculated patterns.

APPLICATION OF THE BWA TECHNIQUE TO EXPERIMENTAL XRD PATTERNS

Fifteen samples representing the full range of I–S expandability were studied by the BWA technique. Expandability of the samples was determined according to Środoń (1980, 1984). The same patterns were used to develop the modified integral width method (Drits et al. 1997). K-saturated samples were dehydrated by heating overnight at 300 °C and then were X-rayed in a dry atmosphere. This procedure, performed under the low relative humidity conditions of Boulder, Colorado, was found sufficient to remove XRD peak broadening caused by swelling interlayers. Dehydration was confirmed by observing that the 002 peak was narrower than the 003 (002 broadening is most sensitive to the presence of 1-water layer smectite) and that the mean $d(001)$ values calculated from the 002, 003 and 005 were nearly identical (the mean deviation from the mean thickness value did not exceed ±0.008 Å for 13 samples and ±0.012 Å for the other 2).

The progression in a BWA-MudMaster analysis for K-saturated, dehydrated Zempleni clay (Viczián 1997), which prior to dehydration was a 15% expandable, $R > 1$ ordered mixed-layer I–S, is presented in Figures 5, 7 and 9 for the 001 reflection. The flipped, undistorted interference function (Figure 5C) was subjected to Fourier analysis (Equation [14]), and the Fourier coefficients, $H(n)$, were plotted against CSD thickness (Figure 7A). Extrapolation of the steepest slope of this curve yields and extrapolated mean ($\bar{T}_e$) of 10.5 nm. The second derivative of this curve (Equation [15]) yields the thickness distribution (Figure 7B) from which the distribution mean ($\bar{T}_d$) was calculated and found also to equal 10.5 nm. If there is no experimen-

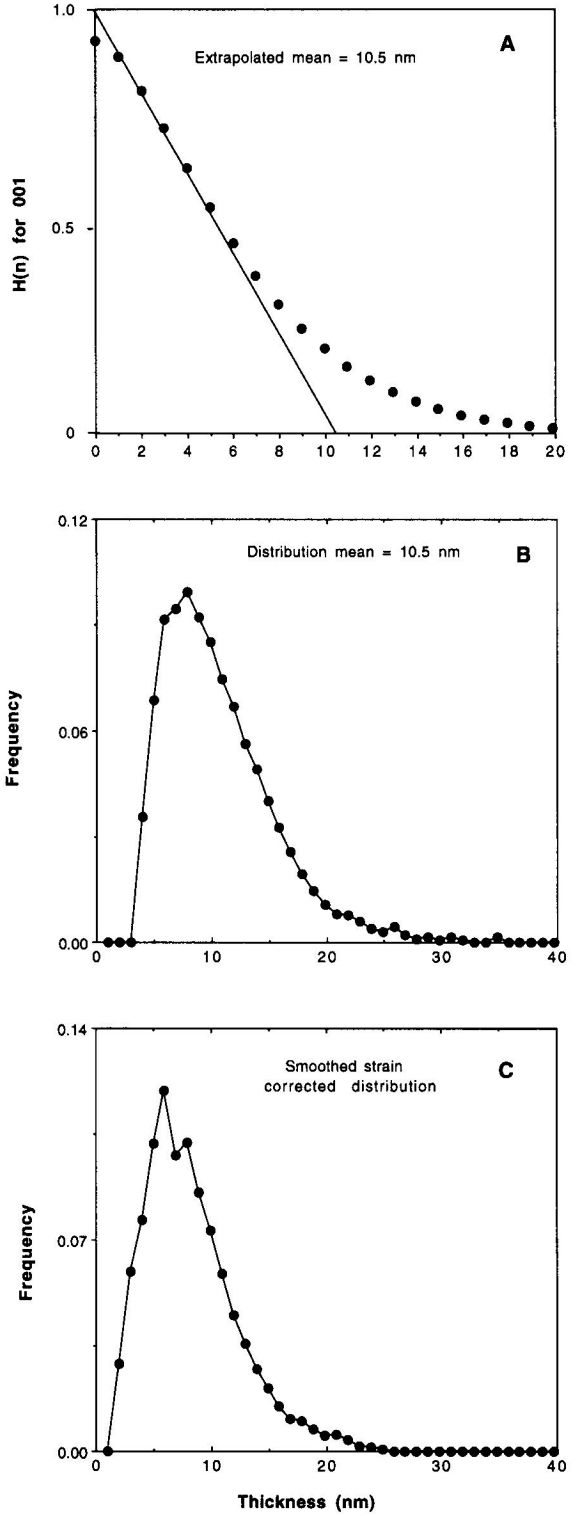

Figure 7. BWA analysis of K-saturated, dehydrated Zempleni sample. See Figure 5 for the XRD data. A = BWA method for determining the extrapolated mean ($\overline{T}_e$); B = crystallite thickness distribution calculated from the curve in A (no smoothing); C = crystallite thickness distribution calculated from Fourier coefficients that have been corrected for strain (smoothing power of 3).

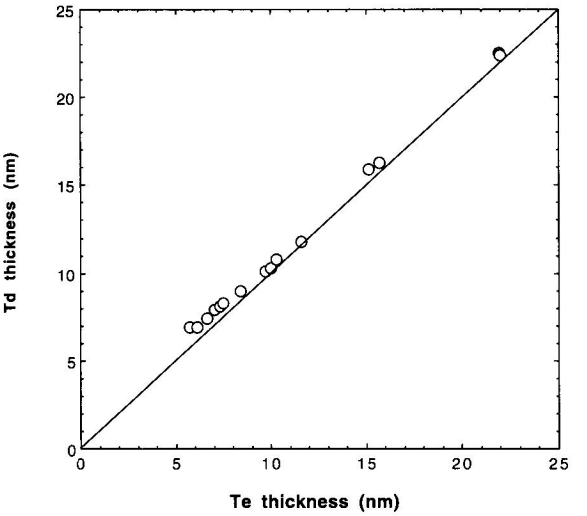

Figure 8. Mean thicknesses for the samples listed in Table 3 determined by extrapolation of Fourier coefficients (T_e; see Figure 7A) compared with those determined from the distributions (T_d; see Figure 7B) for the 001 reflection.

tal error, the means calculated by both approaches should be equal to each other, as is generally the case for the 001 reflection (Figure 8). However, the extrapolated mean is the more accurate and stable mean, because the distribution mean is sensitive to the maximum n used in the calculation, to the smoothing power (smoothing tends to increase $\overline{T}_d$ with respect to $\overline{T}_e$) and to the cutoff value used for the distribution, whereas the extrapolated mean is insensitive to changes in these parameters.

By analyzing more than 1 reflection order, the mean and the distribution can be corrected for strain broadening, which does not significantly affect the 001 and 002 reflections, but which may affect higher orders. Logarithms of Fourier coefficients for the 001, 002, 003 and 005 reflections (Equation [27]) are plotted against the square of the reflection order (l^2) for a range of n's (Figure 9A). The intercepts of these lines on the Y-axis yield the strain-corrected Fourier coefficients, $H(n)$, which then can be used to determine the mean thickness and thickness distribution, as in Figures 7A and 7B. The slopes of these lines yield the mean square of the strain ($\overline{\sigma_n^2} = n\overline{\sigma_1^2}$) for each n. If the ratios $\overline{\sigma_n^2}/n$ are constant, then strain (ϵ_l, in Å units) has a Gaussian distribution (Figure 9C) with a standard deviation $(\overline{\sigma_1^2})^{1/2}$. Correction of the Fourier coefficients for strain broadening yields good mean thickness values (as will be discussed), but may distort thickness distributions. However, if smoothing is applied to the strain-corrected Fourier coefficients (smoothing power = 3 in the MudMaster program), then a distribution is recovered that is similar to that found from the 001 reflection (Figure 7C).

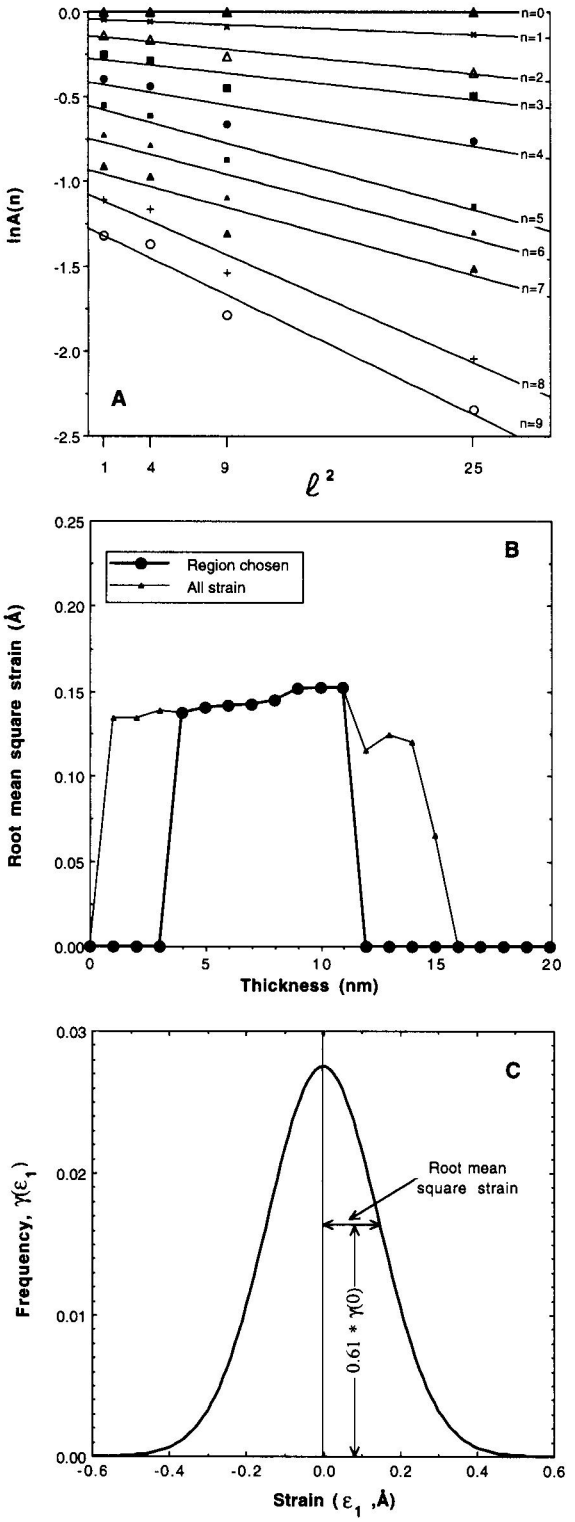

Figure 9. Strain determinations for the Zempleni sample made according to BWA theory. See Figures 5 and 7 for more information concerning this sample. A = plot used to determine the mean square of the strain ($\overline{\varepsilon_1^2}$) as a function of n; B = the plateau in the root mean square strain data indicates that the strain (ϵ_1) has a Gaussian distribution; C = Gaussian strain (ϵ_1, in Å) distribution ($\gamma(\epsilon_1)$; see Equation [24]) for this sample.

Table 2. Parameters of crystallite thickness distributions measured by the BWA method and by the integral peak width method (Drits et al. 1997) from an XRD pattern of a K-exchanged and dehydrated sample of almost nonswelling illite (SG1). A smoothing power of 1 was used for the BWA distributions.

Reflection	$\overline{T}_e$ (nm)	$\overline{T}_d$ (nm)	$\overline{T}_i$ (nm)	α	β^2	$Id(00l)$ (Å)
001	21.9	22.1	18.7	3.006	0.181	10.026
002	24.3	24.4	19.2	3.082	0.229	10.022
003	18.4	21.6	19.0	2.945	0.284	10.008
004	21.7	22.7	17.4	3.037	0.179	10.004
005	19.0	19.9	15.6	2.861	0.278	10.010

Key: See Table 1 for explanation of symbols.

The BWA technique was further tested using sample SG1, an illite that in its natural state contains almost no swelling interlayers. Results (Table 2) indicate that all of the first 5 reflections can be used to determine $\overline{T}_e$ (mean determined by extrapolation), $\overline{T}_d$ (mean determined from the distribution), α and β^2. The means indicate that strain broadening is minimal, because such broadening would tend to regularly decrease $\overline{T}$ with increasing reflection order. Nearly identical results were found when intensity data were corrected for the presence of $K\alpha_2$ radiation. Another pure illite (Kaube) gave similar results for strain analysis, suggesting that strain is minimal within fundamental illite particles (Nadeau et al. 1984), although it is present in dehydrated K-smectite interlayers, as will be discussed below.

Results obtained for 00l reflections from all of the dehydrated samples are presented in Table 3. Area-weighted mean thicknesses obtained from an integral peak width study ($\overline{T}_i$) of the same XRD patterns (Drits et al. 1997) are close to those obtained by the BWA method (Tables 2 and 3 and Figure 10). Our data set does not allow us to evaluate the accuracy of BWA measurements of β^2 for natural samples.

Mean thicknesses for fundamental illite particles (N) can be calculated from mean thicknesses for the dehydrated mixed-layer crystallites ($\overline{T}$) and expandability (%S) (after Drits et al. 1997):

$$N = \frac{100\overline{T}}{(\overline{T} - 1)(\%S) + 100} \quad [34]$$

Values of N calculated using mean thicknesses obtained for 001 reflections from the BWA compare well with those determined from thicknesses obtained by the integral peak width method (Figure 11).

All K-dehydrated samples were analyzed for strain (layer thickness fluctuations) using various combinations of the 001, 002, 003 and 005 reflections. Calculations that used all 4 peaks produced the most reliable results. Strain corrected values for $\overline{T}_e$ obtained by correcting $\overline{T}_e$ of the 005 reflection for strain ($\overline{T}_c$), calculated using the 001, 002, 003 and 005 reflections,

Table 3. Parameters of crystallite thickness distributions measured by the BWA (using a smoothing power of 1) and by the integral peak width methods from 00*l* reflections of XRD patterns of K-exchanged and dehydrated samples. Units are in nm unless otherwise indicated.

Sample	Nfix	N	%S	$\overline{T}_i$ 001	$\overline{T}_e$ 001	$\overline{T}_e$ 002	$\overline{T}_e$ 003	$\overline{T}_e$ 005	$\overline{T}_e$ 005	$(\overline{\sigma_1^2})^{1/2}$
Kaube	45.0	22.0	0	18.1	22.0	20.3	16.4	16.0	21.6	0.061
SG1	11.1	15.4	2	18.7	21.9	24.3	18.4	19.0	23.3	0.049
RM30	10.0	11.8	2	13.4	15.1	14.5	13.2	10.7	15.3	0.099
M11	5.3	7.6	5	9.5	11.6	10.5	8.3	7.9	10.6	0.114
LF10	6.8	8.3	6	13.3	15.7	14.6	12.2	9.9	15.7	0.113
M8	4.1	5.5	7	7.2	8.4	7.8	5.9	5.6	8.2	0.138
RM8	6.3	5.2	10	8.3	9.7	8.0	6.9	6.5	8.6	0.124
RM35A	5.6	4.8	12	8.2	10.0	7.6	6.2	6.1	8.7	0.104
Zempleni	4.5	4.3	15	8.9	10.5	10.1	7.3	6.0	9.9	0.145
T9	2.72	3.1	20	5.6	6.6	5.6	4.3	3.8	6.0	0.177
M10	2.23	2.4	31	5.4	6.1	5.6	4.3	3.7	5.7	0.204
Ch5	1.96	2.2	37	6.2	7.5	6.7	5.0	4.3	7.1	0.178
MB	1.82	2.2	38	7.1	7.3	6.2	4.6	3.7	6.7	0.228
MD	1.15	1.1	88	5.9	5.7	4.9	3.7	3.1	5.5	0.268
2M9	1.09	1.1	88	6.0	7.0	5.6	3.4	3.4	6.7	—

Key: Nfix = thickness of fundamental illite particles calculated by the fixed cation method (Środoń et al. 1992); N = thickness of fundamental illite particles calculated by Equation [34], using $\overline{T}_e$ for the 001 reflection and %S (percentage of smectite interlayers); $\overline{T}_e$ = strain corrected thickness extrapolated from the 001, 002, 003 and 005 refections; and $(\overline{\sigma_1^2})^{1/2}$ = root mean square of the strain calculated from a combination of the 001, 002, 003 and 005 XRD reflections. Remaining symbols are explained in Table 1. The samples have been described in Środoń et al. 1986, Eberl et al. 1987, Środoń et al. 1992 and Środoń and Elsass 1994.

compare closely with those not corrected for strain determined from the 001 and 002 reflections (Table 3), indicating that the effect of strain on $\overline{T}_e$ was removed completely for the 005 reflection and that the 001 and 002 reflections can be used to determine $\overline{T}$ without correction for strain. However, without the strain correction, $\overline{T}$ measured from 005 peak can be underestimated by up to 50% for the most smectitic samples. As was mentioned previously, removal of strain may distort CSD distributions. Therefore, whereas strain-corrected measurements can be used to determine $\overline{T}$ and $(\overline{\sigma_1^2})^{1/2}$ (the root mean square of the strain), reliable CSD thickness distributions can only be obtained from 001 or 002 reflections that have not been corrected for strain.

Plots of $(\overline{\sigma_1^2})^{1/2}$ versus thickness (for example, Figure 9B) indicate that $(\overline{\sigma_1^2})^{1/2}$ is independent of thickness, thereby confirming the Gaussian distribution of strain (Equation [27]) for K-dehydrated I–S. Values of $(\overline{\sigma_1^2})^{1/2}$

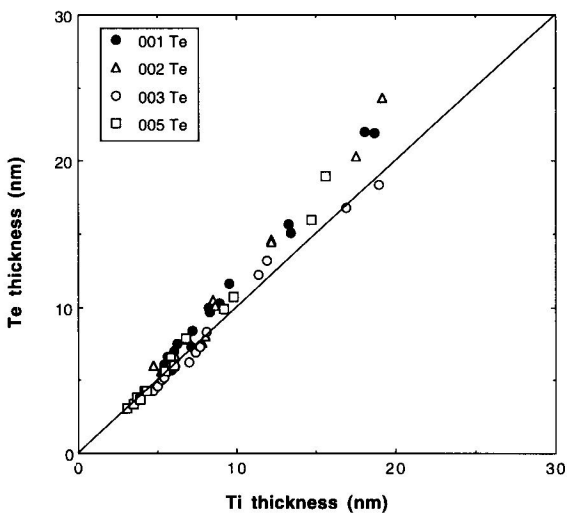

Figure 10. Relation between mean thicknesses measured by the BWA extrapolation method (T_e) and the integral peak breadth method (T_i; Drits et al. 1997) for 5 reflection orders. Data from Table 3.

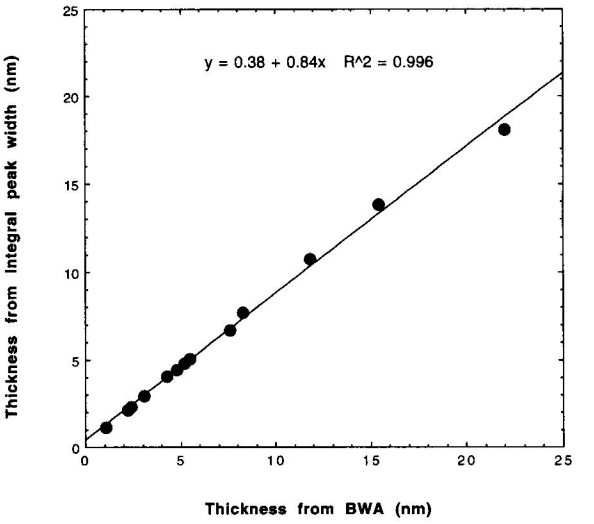

Figure 11. Relation between fundamental illite particle thicknesses calculated integral peak width thicknesses ($\overline{T}_i$) and expandability, and from BWA thickness ($\overline{T}_e$) and expandability using Equation [34].

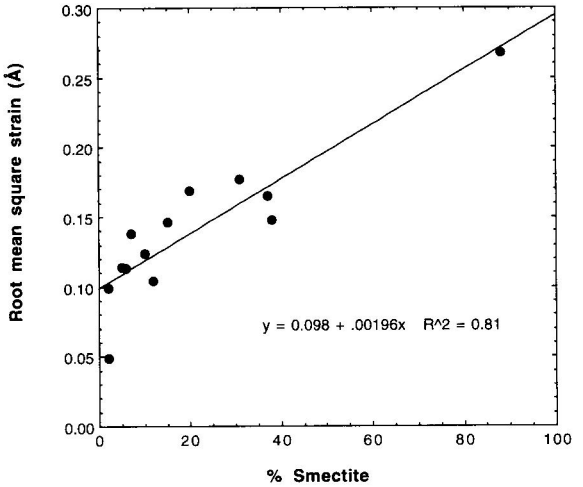

Figure 12. Relation between $(\overline{\sigma_i^2})^{1/2}$, measured from dehydrated I–S, and percent smectite layers, measured from glycol-solvated samples prior to dehydration.

range from 0.049 to 0.268 Å (Table 3) and correlate positively with the percentage of smectite layers (Figure 12).

SUMMARY AND CONCLUSIONS

The MudMaster program (Eberl et al. 1996) was developed to study crystallite thickness distributions and strain in minerals, particularly in clay minerals, by the BWA method. Therefore the program contains several features that differ from commercially available programs designed to study metals. These features include: the analysis of raw data, rather than modeled XRD peaks, so that actual CSD distributions can be extracted from peak shape; the removal of the LpG^2 contribution to the XRD intensities, a contribution that can distort peak shapes for clays; and the flipping of interference function peaks that are situated too closely to zero values for the LpG^2 function.

The BWA method has been applied successfully to study crystallite thickness distributions for illites and I–S up to a mean thickness of about 20 nm, using both calculated and natural samples. Crystallite size distributions for I–S, which can be studied by X-raying K-saturated, dehydrated samples, generally can be approximated by lognormal functions. Independent verification of the accuracy of the XRD measurements was obtained by comparing the mean thickness of the fundamental particles calculated from $\overline{T}_e$ and expandability (Equation [34]), with the mean thickness calculated from $\overline{T}_i$ and expandability (Equation [34], Table 3 and Figure 11).

K-saturation and dehydration of I–S leads to strain broadening for higher-order reflections. The effects of this broadening on measured $\overline{T}$ can be avoided by analyzing the 001 or 002 reflections, or by correcting the Fourier coefficients of the higher-order reflections for strain. Values for the root mean square of the strain increase with increasing expandability and follow a symmetric (Gaussian) distribution. We speculate that strain is induced by 2 phenomena: 1) K ions located in dehydrated smectite interlayer space in positions outside of the ditrigonal holes in the tetrahedral sheets, thereby making the *d*-spacing larger than that of illite; and 2) a deficiency of K ions in other areas of the same interlayer, which makes the spacing smaller than that of illite.

ACKNOWLEDGMENTS

This research was made possible thanks to financial support from the USGS to V. Drits and J. Środoń. Special thanks to R. Krushensky and P. Hearn of the Office of International Geology. We thank J. Neil, R. Nüesch and R. Pollastro for reviewing the initial manuscript. The use of trade names is for identification purposes only and does not constitute endorsement by the U.S. Geological Survey.

REFERENCES

Árkai P, Merriman RJ, Roberts B, Peacor DR, Tóth M. 1996. Crystallinity, crystallite size and lattice strain of illite–muscovite and chlorite: Comparison of XRD and TEM data for diagenetic to epizonal pelites. Eur J Mineral 8:1119–1137.

Bertaut MF. 1949. Étude aux rayons X de la répartition des dimensions des cristallites dans une poudre cristalline. CR Acad Sci Paris 228:492–494.

Bertaut MF. 1950. Raies de Debye-Scherrer et répartition des dimensions des domaines de Bragg dans les poudres polycristallines. Acta Crystallogr 3:14–18.

Drits VA, Środoń J, Eberl DD. 1997. XRD measurement of mean illite crystallite thickness: Reappraisal of the Kubler index and the Scherrer equation. Clays Clay Miner 45:461–475.

Drits VA, Tchoubar C. 1990. X-ray diffraction by disordered lamellar structures. Berlin: Springer-Verlag. 371 p.

Eberl DD, Blum A. 1993. Illite crystallite thickness by X-ray diffraction. In: Reynolds RC Jr, Walker JR, editors. CMS Workshop Lectures, Vol. 5, Computer applications to X-ray powder diffraction analysis of clay minerals. Boulder, CO: Clay Miner Soc. p 124–153.

Eberl DD, Drits V, Środoń J, Nüesch R. 1996. MudMaster: A program for calculating crystallite size distributions and strain from the shapes of X-ray diffraction peaks. USGS Open File Report 96-171. 44 p.

Eberl DD, Środoń J. 1988. Ostwald ripening and interparticle diffraction effects for illite crystals. Am Mineral 73:1335–1345.

Eberl DD, Środoń J, Kralik M, Taylor B, Peterman ZE. 1990. Ostwald ripening of clays and metamorphic minerals. Science 248:474–477.

Eberl DD, Środoń J, Lee M, Nadeau PH, Northrop HR. 1987. Sericite from the Silverton caldera, Colorado: Correlation among structure, composition, origin, and particle thickness. Amer Mineral 72:914–934.

Gangulee A. 1970. Separation of the $\alpha_1 - \alpha_2$ doublet in X-ray diffraction profiles. J Appl Cryst 3:272–277.

Guinier A. 1964. Théorie et technique de la radiocristallographie. Chap 13: Diffraction par les réseaux cristallins imparfaits. Paris: Dunod. p 490–636.

James RW. 1965. The optical properties of the diffraction of X-rays. Vol. II, The crystalline state. Bragg L, series editor. Ithaca: Cornell Univ Pr. 664 p.

Klug HP, Alexander LE. 1974. X-ray diffraction procedures for polycrystalline and amorphous materials, 2nd ed. New York: J Wiley. 966 p.

Kodama H. 1965. Crystal distortion of sericite. Clay Sci 2: 121–131.

Kodama H, Gatineau L, Méring J. 1971. An analysis of X-ray diffraction line profiles of microcrystalline muscovites. Clays Clay Miner 19:405–413.

Lanson B, Kubler B. 1994. Experimental determination of the coherent scattering domain size distribution of natural mica-like phases with the Warren-Averbach technique. Clays Clay Miner 42:489–494.

Maire J, Mering J. 1960. Croissance des dimensions des domaines cristallins au cours de la graphitation du carbons. Proc 4th Conf Carbon. New York: Pergamon Pr. p 345–350.

Moore DM, Reynolds RC Jr. 1989. X-ray diffraction and the identification of clay minerals. New York: Oxford Univ Pr. 332 p.

Nadeau PH, Wilson MJ, McHardy WJ, Tait JM. 1984. Interstratified clay as fundamental particles. Science 225:923–935.

Reynolds RC Jr. 1985. NEWMOD©, a computer program for the calculation of one-dimensional diffraction patterns of mixed-layered clays. R. C. Reynolds, Jr., 8 Brook Dr., Hanover, NH 03755.

Reynolds RC Jr. 1986. The Lorentz-polarization factor and preferred orientation in oriented clay aggregates. Clays Clay Miner 34:359–367.

Reynolds RC Jr. 1989. Diffraction by small and disordered crystals. In: Bish DL, Post JE, editors. Modern powder diffraction. Washington, DC: Miner Soc Am. p 145–181.

Siemens. 1990. Diffrac 5000 powder diffraction evaluation software reference manual, release 2.2, part no. 269-00200. Siemens Analytical Instruments, Inc., 6300 Enterprise Lane, Madison, WI 53719. p 16.15.

Środoń J. 1980. Precise identification of illite/smectite interstratifications by X-ray powder diffraction. Clays Clay Miner 28:401–411.

Środoń J. 1984. X-ray diffraction of illitic materials. Clays Clay Miner 32:337–349.

Środoń J, Elsass F. 1994. Effect of the shape of fundamental particles on XRD characteristics of illitic minerals. Eur J Mineral 6:113–122.

Środoń J, Elsass F, McHardy WJ, Morgan DJ. 1992. Chemistry of illite-smectite inferred from TEM measurements of fundamental particles. Clay Miner 27:137–158.

Środoń J, Morgan DJ, Eslinger EV, Eberl DD, and Karlinger MR. 1986. Chemistry of illite/smectite and end-member illite. Clays Clay Miner 34:368–378.

Stokes AR. 1948. A numerical Fourier-analysis method for the correction of widths and shapes of lines on X-ray diffraction photographs. Proc Phys Soc (London) A61:382–391.

Viczián I. 1997. Hungarian investigations on the "Zempleni" illite. Clays Clay Miner 45:114–115.

Warren BE, Averbach BL. 1950. The effect of cold-work distortion on X-ray patterns. J Appl Phys 21:595–599.

(Received 2 January 1997; accepted 15 April 1997; Ms. 97-001)